ISFV13 - 13th International Symposium on Flow Visualization
FLUVISU12 - 12th French Congress on Visualization in Fluid Mechanics
July 1-4, 2008, Nice, France

VISUALIZING THE FLOW INDUCED BY AN AIR CURTAIN OVER A MANNEQUIN USING STEREO PARTICLE IMAGE VELOCIMETRY

Frank K. Lu, John E. Fernandes
University of Texas at Arlington, Arlington, Texas 76019, USA

KEYWORDS:
Main subject(s): *Environmental flow*
Fluid: *Aerodynamics*
Visualization method(s): *Stereo particle image velocimetry*
Other keywords: *Air curtain, mannequin*

ABSTRACT: *The flow of an air curtain mounted above a doorway in which was placed a mannequin was studied using stereo particle image velocimetry. The study revealed that the interference of the air curtain flow was limited to a region near the doorway. The air curtain flow stagnates around the top surfaces of the mannequin. A high level of turbulence also existed in this region. The turbulence diminished rapidly past the mannequin and increased in a thin region near the floor as the flow entered the floor vents.*

1 Introduction

Air curtains are highly versatile devices that are used to provide a dynamic barrier for easy movement of people and materials. For a historical review of innovative applications, see [1]. Most of the early studies of air curtains emphasized performance parameters of the installed devices alone, usually with highly idealized configurations [2–7]. More recently, advanced experimental and computational techniques have been applied to facilitate the study of more complex configurations [8–20], with the realization that rectangular jets cannot be properly considered as two-dimensional planar jets [21,22].

Much of the literature on air curtains has been in refrigeration where the emphasis has been in reducing the entrainment of warm ambient air and in improving energy efficiency, per the above-cited references. In addition, there has been a longstanding interest in using air curtains for isolation [23–33] and they have been proposed for explosives detection portals [34]. Unfortunately, practically all of the reported studies involve the bare air curtain flow. Therefore, further understanding of air curtains for critical demands necessitates studying such flows subjected to disturbances [35–38]. The presence of a moving subject, such as a human, poses tremendous difficulties for experiment or numerical simulation. Instead, further understanding can nonetheless be achieved by studying the flow past a stationary mannequin, which is the aim of the present study.

There is precedence in using mannequins for studying ventilation and natural convection associated with human activities. References [39–42] are recent examples of the use of heated mannequins to simulate the actual thermal state of humans. In some situations, unheated mannequins are used, for example [43– 45]. A more specific example of an air curtain flow with a mannequin can be found in [46]. In general, unheated mannequins are used in situations where a forced convective flow exists.

Representing a human being by a mannequin may be problematic since the actual thermal condition is not properly modeled. A recent study of the human thermal plume showed that the maximum plume velocity was 0.24 m/s [47] Comparing this against the maximum velocity of the flow leaving the air curtain of the present study of 5.8 m/s [20], one can conclude that the human plume is negligible. Thus, the isothermal mannequin is deemed adequate for the present study.

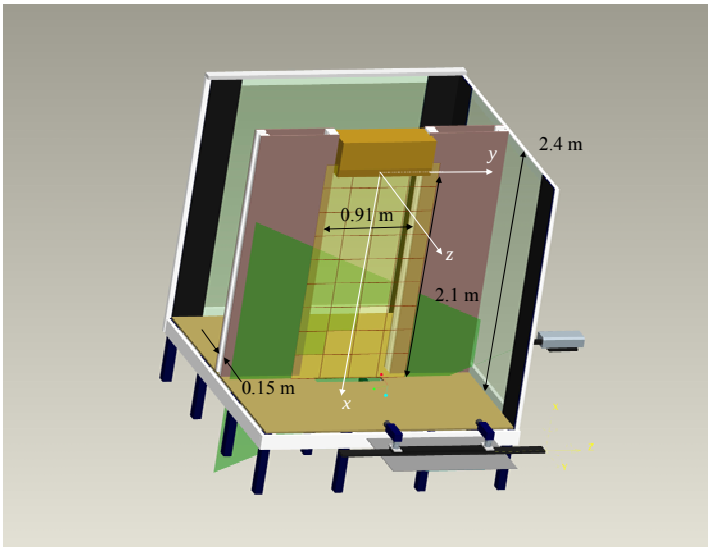

Fig. 1. Cutaway view of test cabin.

An alternate justification of an isothermal mannequin can be made based on buoyancy considerations. Buoyancy effects are negligible for low values of the Richardson number $Ri = \left(\rho_{amb} - \rho_{jet}\right)gh \big/ \rho_{amb} V_{jet}^2$. In a study of cold wall jets pertinent to air curtains [12], the justification for an isothermal assumption was that the low value of the Richardson number of 0.3. For the present case, a clothed human will have an average surface temperature of 26.6°C [47]. With an ambient temperature of 20°C, a characteristic height of 2 m and a jet velocity of about 6 m/s, the Richardson number for the present experiment is about 0.01, that is, practically zero, thus amply justifying the use of an isothermal mannequin.

2 Experimental Method

The experimental method has been presented in [20] and thus will only be briefly mentioned here. A 2.4 m^3 test cabin, raised 0.6 m from the laboratory floor and partitioned midway by a 0.15 m thick wall, with a 0.91 m wide × 2.1 m doorway, is shown schematically in Fig. 1. The facility was raised 0.6 m from the laboratory floor to accommodate ducting. A Fantech Model AC3600 air curtain was mounted on top of the doorway. This air curtain is capable of delivering a maximum flow velocity of 10.3 m/s and a maximum flow rate of 22.5 m^3/min. The entire air curtain exhaust housing was locked to deliver a vertical air curtain downward. The exhaust of the air curtain was directed through a grilled vent comprising of a grid of six rows of 25 rectangular openings, each 30 mm long by 10 mm wide, totaling 0.0444 m^2.

The flow was produced by a fan in the air curtain and captured by two floor vents directly below the air curtain and separated from each other by 25.4 mm. The vents were covered by registers, each 101.6 wide by 304.8 mm long. The total open area of the floor vents was approximately equal to the open area of the air curtain exhaust vent. Upon passing the floor vent, the air entered a 0.0084 m^3 plenum. The air then traveled through a 305 mm diameter air conditioning duct which redirected it to the cabin's roof, entering the diffuser which was located approximately 3.5 ft behind the air curtain unit. Next, the air passed through the diffuser to smooth the flow. After the diffuser, the air traveled back to the front portion of the air curtain as mentioned above. An airtight circulation system was thus set up. The air curtain fixture was offset to the side of the doorway nearer to the SPIV system to enable the bulk of the flow to be mapped.

A commercial, white male mannequin (Rudy1/F, Mondo Mannequins, New York) was placed in the doorway, as shown in Fig. 2. The mannequin is 1.84 m tall. Other, pertinent dimensions include a chest that is 356 wide and 203 mm thick (this being the thickest part of the mannequin). The waist is 318 mmwide and 165 mm thick. The widest dimension of the mannequin is 546 mm measured from the knuckles of both hands. The mannequin was dressed with a black tracksuit made of cotton with the head, hands and feet exposed. The original stand was removed to avoid interference with the floor registers. The center of the mannequin was 77.8 mm ahead of the leading edge of the doorway. The leftmost position of the mannequin was 443.9 mm from the left post of the doorway while the rightmost position of the mannequin was 466.1 mm from the right post. The slight asymmetry was due to the slight offset of the air curtain to accommodate its switch at the right side of the doorway.

Fig. 2. Mannequin in test cabin.

A LaVision FlowMaster 3D SPIV system was used for SPIV. A cylindrical lens with a focal length of $f = -10$ mm spread a beam of light from a New Wave Research Solo 120 Nd:YAG double-pulsed laser into a 2.5 mm thick sheet. This allowed a working distance of 2 m which fulfilled the distance requirement needed for the laser to properly illuminate the measurement area. The lasers were pulsed at 5 Hz at 2 × 120 mJ/pulse, with a pulse duration of 11 ms. The images were captured by two Flow Master 3S ImagerIntense/ImagePro ICCD cameras with 1376 × 1040 pixel resolution and a 12 bit dynamic range. Other major components of the imaging system included a frame grabber, control electronics and a host computer running the DaVis 7.1 PIV data acquisition and processing software. Data were stored in a 750 GB hard drive.

A LaVision V-Z Droplet Seeder producing droplets of extra virgin olive oil with an estimated mean diameter of 1 μm was run for 15 s with the air curtain turned on. After turning off the seeder, the air curtain was run for a further minute to distribute the seed material. Sufficient seed material was then produced without saturating the cameras. The droplet concentration decreased due to absorption into the wooden structure and through tiny leaks. However, sufficient seed was available for 45 minutes which was adequate for surveying an entire plane.

2.3 Experimental Procedure

The surveys were in vertical planes parallel to the doorway. The cameras were mounted on a lift system that allowed them to be aligned parallel with the survey planes in the lateral displacement configuration [48]. The separation between the two cameras was 815 mm. Each camera subtended the same angle with the light sheet. The separation of 815 mm yielded a half-angle between each camera and the center of the image of 12.45 to 17.46°, which was within the recommendations of [11], thereby minimizing off-axis error in the horizontal plane.

Lu and Pierce [20] reported a comprehensive survey of six planes of a bare air curtain flow. That study showed that the air curtain flow was confined to a narrow region. Therefore, in this study, only three

planes were surveyed. The same numbering system as [20] was kept to be consistent. In the present study, surveys were made of planes 1, 3 and 4. The locations of these planes relative to the camera plane are listed in Table 1. Plane 1 was located at the longitudinal axis of the air curtain. Mannequin blockage and limited laboratory access allowed only the right side, i.e., the mannequin's left, to be surveyed.

With only a small common area being captured by the camera pair, a survey of an entire plane required that the ensemble-averaged images of individual common areas be patched together. The actual distribution of the rectangular patchwork is found in Table 1. Due to perspective, the rectangles diminish as one approached the cameras. The uncertainties in the images are $\Delta x \approx 1$ mm, $\Delta y \approx 2$ mm and $\Delta z \approx 4$ mm [20].

Table 1. Rows and rectangles per survey plane.

Plane	Location of plane from camera plane (mm)	No. of rows and rectangles	Size of individual rectangle (mm^2)	Total image size (m^2)
1	1846.5	10 × 2	299.6 × 222.9	0.574 × 1.968
3	1675.0	10 × 4	275.4 × 198.6	1.123 × 2.000
4	1600.0	10 × 4	263.1 × 195.8	1.095 × 1.971

Based on [20], four hundred stereo images were taken at each location in order to obtain ensemble-averaged statistics for the mean and turbulent flow quantities. After the ensemble has been obtained, the cameras were then moved horizontally to obtain images from the next rectangle and so forth to collect data for an entire row. Upon completing a given row, the lift moved the camera to the next row and the process was repeated. The dataset for an entire plane was then processed by DaVis to yield ensemble statistics of the velocity field. DaVis merged the data of each rectangle to yield ensemble data of the entire plane. The topmost row (No. 8) was designated as the datum row. The entire process of acquiring the SPIV images and processing the data for each plane took about 16 hours.

3 Results

3.1 Streamlines

The ensemble-averaged, in-plane streamline maps are shown in Fig. 3. The mannequin silhouette or outline is included in the maps as appropriate while the doorway location is shown by the yellow frame. Moreover, the SPIV system was unable to access a thin region at the exit of the air curtain. This region is blocked off as a black rectangle in the maps. This inaccessible region varied slightly from plane to plane.

Figure 3a shows a distinct shear layer demarcating the air curtain flow from the still ambient environment. Figures 3b and c show erratic flow just slightly away from the mannequin. This flow, which is extremely slight as will be shown later, appears to be due to entrainment by the air curtain. A similar erratic flow behavior was seen in the bare air curtain flow [20]. It appears that the mannequin disturbed the air curtain flow substantially in Plane 1 but that the disturbance is not significant in Planes 3 and 4.

3.2 Velocity Profiles

The ensemble-averaged, in-plane velocity maps are shown in Fig. 4. These velocity maps complement the ensemble-averaged streamline maps of Fig. 3 and help in understanding how the presence of the mannequin affects the air curtain flow. Figure 4a shows that the jet leaving the air curtain was disrupted by the mannequin. The u velocity component directly over the mannequin was reduced as the flow stagnates. The u velocity component was stronger (but at reduced strength compared to the bare air curtain [20]) past the mannequin's head. The three-dimensionality of the flow is also evident in Fig. 4a. Moreover, the mannequin produced regions, especially above the shoulder and to the right of the leg, where the SPIV system was unable to yield good data, as evidenced by disruptions in the velocity profiles in those regions. The air curtain flow diminished in velocity as it approaches the floor. Interestingly, the data showed that large variations in the transverse velocity components appeared at the floor, which can be attributed to the registers covering the floor vents.
The surveys in Planes 3 and 4 showed that the mannequin presented a minor disturbance in those regions (Figs. 4b and c). The transverse velocity components were relatively larger than those for the bare air curtain.

3.2 Turbulence Quantities

Figure 5 shows the turbulent kinetic energy (TKE). The figure shows that the TKE is generally small and negligible except for regions within the air curtain above the mannequin's shoulder and at the floor vents. The flow leaving the air curtain is also turbulent, as is typically found in other air curtains [13]. Figure 5c shows a triangular artifact to the right of the mannequin. This is due to stray scattering from a scratch on the transparent wall. Another artifact that is visible in Figs. 5b and c are dark spots to the right of the mannequin's face and hands. These dark spots are due to laser light reflection from these reflective surfaces even though the laser sheet is shining in planes that do not incident on the mannequin. The DaVis software is unable to interrogate those saturated regions and returned no values. Figure 5 also shows the patchwork of individual interrogation regions that forms the composite maps which was not evident in the maps of mean properties.
The Reynolds stress distributions for plane 1 shows a high region of turbulence as the jet exits the air curtain, as well as at the floor as the flow enters the vents (Fig. 6). The figures reveal a thin region at the interface of the air curtain with the surroundings. Figure 7 shows the $\overline{u'v'}$ Reynolds stress distribution for plane 3. (The other components as well as the Reynolds stress distributions for plane 4 are not shown for brevity.) Figure 7 shows that there is a negligible amount of turbulence within the resolution of the SPIV system, similar to that shown in Figs. 5b and c of the TKE. Similar conclusions can be drawn on the distributions not shown in this paper.

4. Conclusions

The flow from a commercial, off-the-shelf air curtain past a mannequin was visualized using stereo particle image velocimetry. A previously developed patchwork technique for mapping a large region was used. The presence of shiny surfaces of the mannequin caused some regions of the maps to be devoid of useful data.
The study showed that the mannequin, when located directly below the air curtain, disturbed the flow. However, the disturbance was largely confined to the vicinity of the air curtain. The turbulent flow from the air curtain was damped rapidly by the presence of the mannequin.

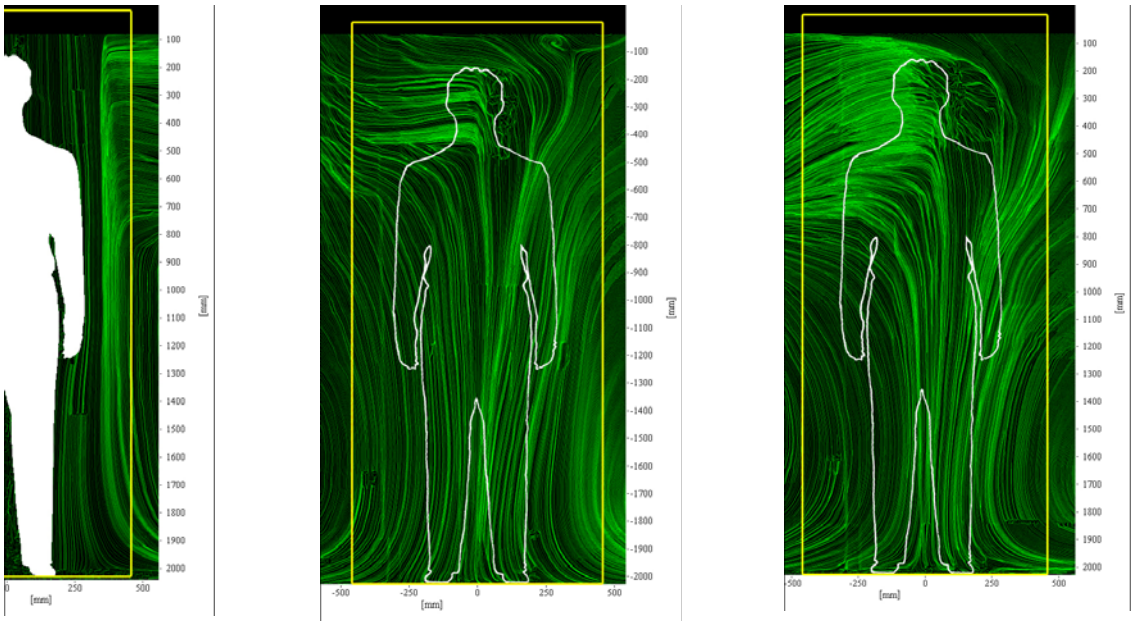

a. Plane 1. b. Plane 3 c. Plane 4.

Fig. 3. Ensemble-averaged streamlines.

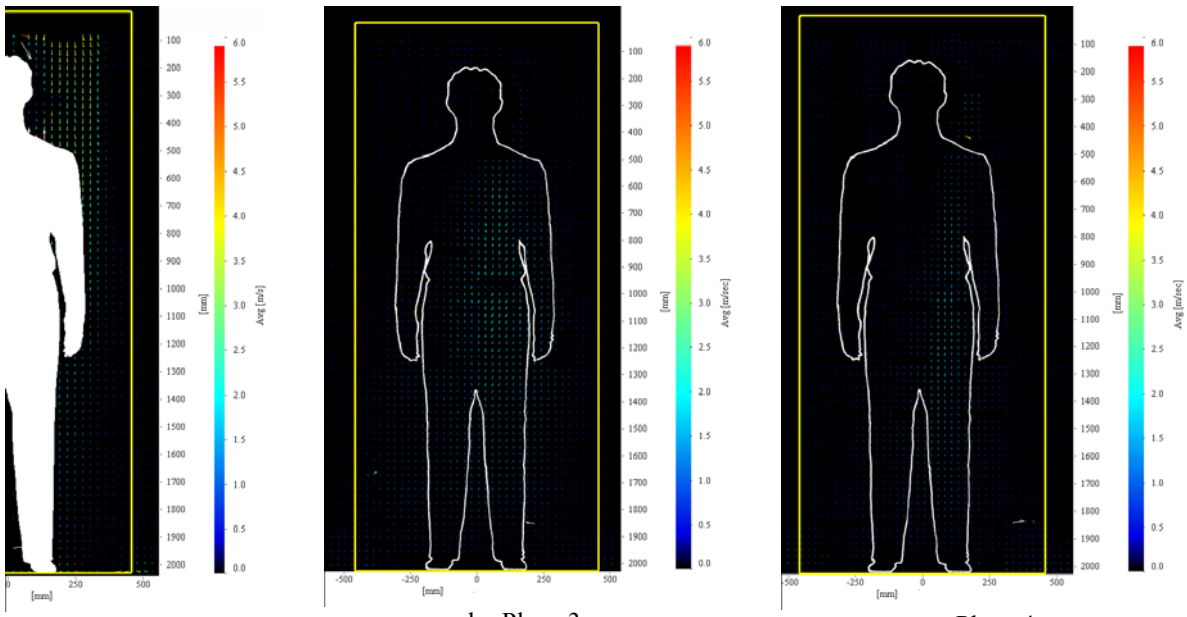

a. Plane 1. b. Plane 3. c. Plane 4.

Fig. 4. Ensemble-averaged velocity maps.

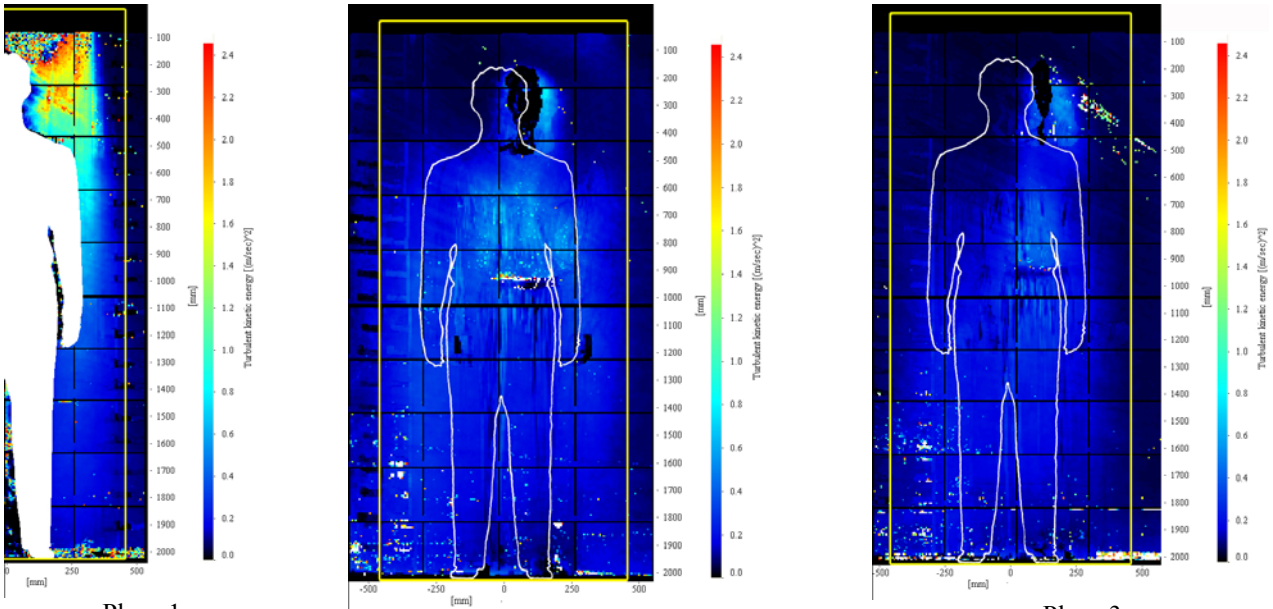

a. Plane 1. b. Plane 2. c. Plane 3.

Fig. 5. Turbulent kinetic energy.

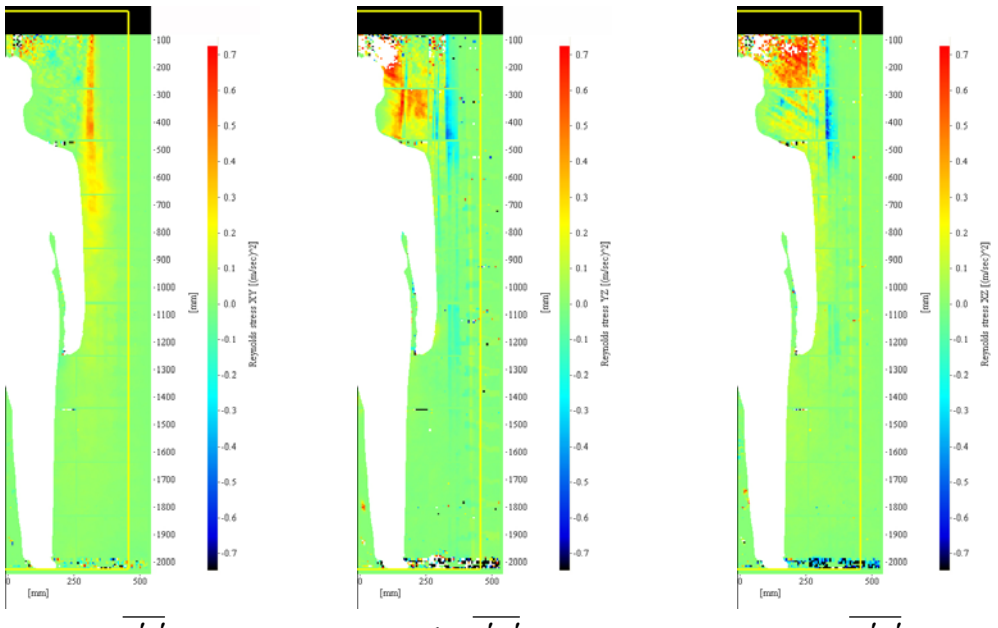

a. $\overline{u'v'}$. b. $\overline{v'w'}$. c. $\overline{w'u'}$.

Fig. 6. Reynolds stresses of plane 1.

5 Acknowledgements

Funding for the SPIV system was a National Science Foundation's Major Research Instrument Grant (No. 0421282). The assistance of Adam Pierce is gratefully acknowledged.

References

1. Etkin B, Goering PLE. Air-curtain walls and roofs–'dynamic' structures. *Philosophical Transactions of the Royal Society of London A*, Vol. 269, No. 1199, pp. 527–543, 1971.
2. Hetsroni G, Hall CW, Dhanak AM. Heat transfer properties of an air curtain. *Transactions of the American Society of Agricultural Engineering*, Vol. 6, pp. 328–334, 1963.
3. Hayes FC, Stoecker WF. Heat transfer characteristics of the air curtain. *ASHRAE Transactions*, Vol. 75, No. 2, pp. 153–167, 1969.
4. Howell RH, Shibata M. Optimum heat transfer through turbulent recirculated plane air curtains. *ASHRAE Transactions*, Vol. 86, No. 1, pp. 188–200, 1980.
5. Lawton E, Howell R. Energy savings using air curtains installed in high traffic doorways. *ASHRAE Transactions*, Vol. 101, No. 2, pp. 136–143, 1995.
6. Navaz H, Dabiri D, Amin M, Faramarzi R. Past, present, and future research toward air curtain performance optimization. *ASHRAE Transactions*, Vol. 111, No. 1, pp. 1083–1088, 2005.

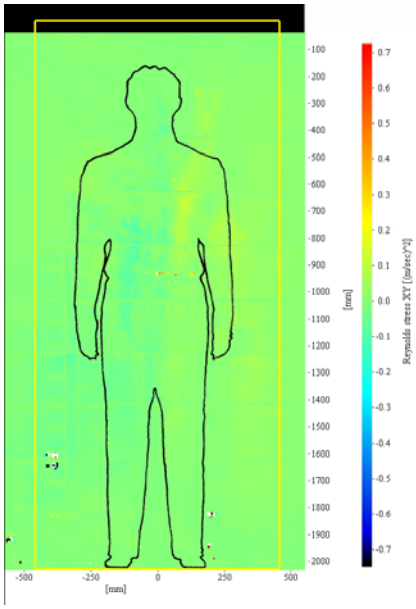

a. .

Fig. 7. Map of $\overline{u'v'}$ in plane 3.

7. Ge YT, Tassou SA. Simulation of the performance of single jet air curtains for vertical refrigerated display cabinets. *Applied Thermal Engineering*, Vol. 21, No. 2, pp. 201–219, 2001.
8. Navaz HK, Faramarzi R, Gharib M, Dabiri D, Modarress D. The application of advanced methods in analyzing the performance of the air curtain in a refrigerated display case. *Journal of Fluids Engineering*, Vol. 124, No. 3, pp. 756–764, 2002.
9. Foster AM, Swain MJ, Barrett R, James SJ. Experimental verification of analytical and CFD predictions of infiltration through cold store entrances. *International Journal of Refrigeration*, Vol. 26, No. 8, pp. 918–925, 2003.
10. Sirén K. Technical dimensioning of a vertically upwards blowing air curtain—part I. *Energy and Buildings*, Vol. 35, No. 7, pp. 681–695, 2003.
11. Sirén K. Technical dimensioning of a vertically upwards-blowing air curtain—part II. *Energy and Buildings*, Vol. 35, No. 7, pp. 697–705, 2003.
12. Bhattacharjee P, Loth, E. Simulations of laminar and transitional cold wall jets. *International Journal of Heat and Fluid Flow*, Vol. 25, No. 1, pp. 32–43, 2004.
13. Field BS and Loth E. An air curtain along a wall with high inlet turbulence. *Journal of Fluids Engineering*, Vol. 126, No. 3, pp 391–398, 2004.
14. Cui J and Wang S. Application of CFD in evaluation and energy-efficient design of air curtains for horizontal refrigerated display cases. *International Journal of Thermal Sciences*, Vol. 43, No. 10, pp 993–1002, 2004.
15. Foster AM, Madge M, Evans JA. The use of CFD to improve the performance of a chilled multi-deck retail display cabinet. *International Journal of Refrigeration*, Vol. 28, No. 5, pp. 698–705, 2005.
16. Navaz HK, Henderson BS, Faramarzi R, Pourmovahed A, Taugwalder F. Jet entrainment rate in air curtain of open refrigerated display cases. *International Journal of Refrigeration*, Vol. 28, No. 2, pp. 267–275, 2005.

17. Costa JJ, Oliveira LA, Silva MCG. Energy savings by aerodynamic sealing with a downward-blowing plane air curtain—a numerical approach. *Energy and Buildings*, Vol. 38, No. 10, pp. 1182–1193, 2006.
18. D'Agaro P, Cortella G and Croce G. Two- and three-dimensional CFD applied to vertical display cabinets simulation. *International Journal of Refrigeration*, Vol. 29, No. 2, pp. 178–190, 2006.
19. Navaz HK, Amin N, Rasipuram SC, Faramarzi R. Jet entrainment minimization in an air curtain of open refrigerated display case. *International Journal of Numerical Methods for Heat and Fluid Flow*, Vol. 16, No. 4, pp. 417–430, 2006.
20. Lu FK, Pierce AJ. Visualizing the flow induced by an air curtain using stereo particle image velocimetry. *Proc ISFV13 – 13th International Symposium of Fluid Visualization*, Paper 234, July 1–4, 2008.
21. Quinn WR. Turbulent free jet flows issuing from sharp-edged rectangular slots: The influence of slot aspect ratio. *Experimental Thermal and Fluid Science*, Vol. 5, No. 2, pp. 203–215, 1992.
22. Deo RC, Mi J, Nathan GJ. The influence of nozzle aspect ratio on plane jets. *Experimental Thermal and Fluid Science*, Vol. 31, No. 8, pp. 545–559, 2007.
23. Huszer RJ. Air curtains for patient isolation. *Journal of the American Medical Association*, Vol. 207, No. 3, pp. 549–551, 1969.
24. Buchberg H, Lilly GP. Model studies of directed sterile air flow for hospital isolation. *Annals of Biomedical Engineering*, Vol. 2, No. 1, pp. 106–122, 1974.
25. Robertson P, Shaw BH. Linear air curtain as a particulate barrier. Journal of Environmental Science 21(3):32–33. 1978.
26. Breum NO, Nielsen BH, Møller Nielsen E, Poulsen OM. Bio-aerosol exposure during collection of mixed domestic waste—an intervention study on compactor truck design. *Waste Management and Research*, Vol. 14, No. 6, pp. 527–536, 1996.
27. Chow WK. Smoke control by air curtain for spaces adjacent to atria. *Journal of Environmental Systems*, Vol. 27, No. 2, pp. 151–162, 1999–2000.
28. Rydock JP, Hestad T, Haugen H, Skaret JE. An isothermal air curtain for isolation of smoking areas in restaurants. In: Air Distribution in Rooms, ROOMVENT 2000, Proc 7th International Conference on Ventilation for Health and Sustainable Environment, Awbi HB (ed.) Elsevier, Amsterdam, 2000.
29. Pavageau M, Nieto EM, Rey C. Odour and VOC confining in large enclosures using air curtains. *Water Science and Technology*, Vol. 44, No. 9, pp. 165–171, 2001.
30. Lee H, Awbi HB. Effect of internal partitioning on indoor air quality of rooms with mixing ventilation—basic study. *Building and Environment*, Vol. 39, No. 2, pp. 127–141, 2004.
31. Li Y, Huang X, Yu ITS, Wong TW, Qian H. Role of air distribution in SARS transmission during the largest nosocomial outbreak in Hong Kong. *Indoor Air*, Vol. 15, No. 2, pp. 83–95, 2004.
32. Hu SC, Chuah YK, Yen MC. Design and evaluation of a minienvironment for semiconductor manufacture process. *Building and Environment*, Vol. 37, No. 2, pp. 201–208, 2002.
33. Carlson DA, Hogsette JA, Kline DL, Geden CD, Vandermeer RK. Prevention of mosquitoes (diptera: culicidae) and house flies (diptera: muscidae) from entering simulated aircraft with commercial air curtain units. *Journal of Economic Entomology*, Vol. 99, No. 1, pp. 182–193, 2006.
34. Hallowell SF. Screening people for illicit substances: a survey of current portal technology. *Talanta*, Vol. 54, No. 3, pp. 447–458, 2001.
35. Havet M, Rouaud O, Solliec C. Experimental investigations of an air curtain device subjected to external perturbations. *International Journal of Heat and Fluid Flow*, Vol. 24, No. 6, pp. 928 930, 2003.
36. Rouaud O, Havet M, Solliec C. Influence of external perturbations on a minienvironment: experimental investigations. *Building and Environment*, Vol. 39, No. 7, pp. 863–872, 2004.
37. Rouaud O, Havet M. Behavior of an air curtain subjected to transversal pressure variations. *Journal of Environmental Engineering*, Vol. 132, No. 2, pp. 263–270, 2006.

38. Flynn MR, Gatano BL, McKernan JL, Dunn KH, Blazicko BA, Carlton GN. Modeling breathing-zone concentrations of airborne contaminants generated during compressed air spray painting. *Annals of Occupational Hygiene*, Vol. 43, No. 1, pp. 67–76, 1999.
39. Xing H, Hatton A, Awbi HB, A study of the air quality in the breathing zone in a room with displacement ventilation. *Building and Environment*, Vol. 36, No. 7, pp. 809–820, 2001. [[heated mannequin]]
40. Lundgren L, Skare L, Lidén C. Tornling G. Large organic aerosols in a dynamic and continuous whole-body exposure chamber tested on humans and on a heated mannequin. *Annals of Occupational Hygiene*, Vol. 50, No. 7, pp. 705–715, 2007.
41. Lee E., Khan JA, Feigley CE, Ahmed MR, Hussey JR. An investigation of air inlet types in mixing ventilation. *Building and Environment*, Vol. 42, No. 3, pp. 1089–1098, 2007.
42. Wang A, Zhang Y, Sun Y, Wang X. Experimental study of ventilation effectiveness and air velocity distribution in an aircraft cabin mockup. *Building and Environment*, Vol. 43, No. 3, pp. 337–343, 2008.
43. Welling I, Andersson I-M, Rosen G, Räisänen J, Mielo T, Marttinen K, Niemelä R. Contaminant dispersion in the vicinity of a worker in a uniform velocity field. *Annals of Occupational Hygiene*, Vol. 44, No. 3, pp. 219–225, 2000.
44. Flynn MR, Sills ED. Numerical simulation of human exposure to aerosols generated during compressed air spray-painting in cross-flow ventilated booths. *Journal of Fluids Engineering*, Vol. 123, No. 1, pp. 64–70, 2001.
45. Nielsen PV, Computational fluid dynamics and room air movement. *Indoor Air*, Vol. 14, No. 7, pp. 134 – 143, 2004.
46. Huang RF, Wu YD, Chen HD, Chen C-C, Chen C-W, Chang C-P, Shih T-S. Development and evaluation of an air-curtain fume cabinet with considerations of its aerodynamics. *Annals of Occupational Hygiene*, Vol. 51, No. 2, pp. 189–206, 2007.
47. Craven BA, Settles GS. A computational and experimental investigation of the human plume. *Journal of Fluids Engineering*, Vol. 128, No. 6, pp. 1251–1258, 2006.
48. Prasad AK. Stereoscopic particle image velocimetry. *Experiments in Fluids*, Vol. 29, No. 2, pp. 103–106, 2000.

6 Copyright Issues

The copyright statement is included in the template and must appear in your final pdf document in the position, style and font size shown below.

Copyright Statement